Quantifying the Magnetic Advantage in Magnetotaxis

M. J. Smith,* P. E. Sheehan,* L. L. Perry,† K. O'Connor,‡ L. N. Csonka,‡ B. M. Applegate,† and L. J. Whitman*
*Chemistry Division, Naval Research Laboratory, Washington, District of Columbia 20375; and †Department of Food Science, and ‡Department of Biological Sciences, Purdue University, West Lafayette, Indiana 47907

ABSTRACT Magnetotactic bacteria are characterized by the production of magnetosomes, nanoscale particles of lipid bilayer encapsulated magnetite, that act to orient the bacteria in magnetic fields. These magnetosomes allow magneto-aerotaxis, which is the motion of the bacteria along a magnetic field and toward preferred concentrations of oxygen. Magneto-aerotaxis has been shown to direct the motion of these bacteria downward toward sediments and microaerobic environments favorable for growth. Herein, we compare the magneto-aerotaxis of wild-type, magnetic *Magnetospirillum magneticum* AMB-1 with a nonmagnetic mutant we have engineered. Using an applied magnetic field and an advancing oxygen gradient, we have quantified the magnetic advantage in magneto-aerotaxis as a more rapid migration to preferred oxygen levels. Magnetic, wild-type cells swimming in an applied magnetic field more quickly migrate away from the advancing oxygen than either wild-type cells in a zero field or the nonmagnetic cells in any field. We find that the responses of the magnetic and mutant strains are well described by a relatively simple analytical model, an analysis of which indicates that the key benefit of magnetotaxis is an enhancement of a bacterium's ability to detect oxygen, not an increase in its average speed moving away from high oxygen concentrations.

INTRODUCTION

Magnetotactic bacteria are a fascinating group of organisms, most of which contain at least one chain of magnetic nanoparticles (magnetosomes) that acts as a single magnetic dipole. The magnitude of the dipole is sufficiently large that the geomagnetic field will direct the cell's migration by overcoming the Brownian forces that would otherwise randomize its motion (1). Most magnetotactic bacteria are obligate microaerophiles or anaerobes and their magnetosome production is correlated to the oxygen concentration in their environment (2,3). Magnetotaxis or magneto-aerotaxis is not a tactile response to a magnetic field gradient, but rather is widely assumed to passively enhance the efficiency of aerotaxis by orienting the response (1,4–6). To date, the means by which the magnetic alignment allegedly enhances the efficiency of aerotaxis has not been examined.

In their aquatic environments, magnetotactic bacteria experience both vertical oxygen gradients and a vertical component in the geomagnetic field (high at the North and South poles decreasing to zero at the equator). It was therefore a natural hypothesis that the magnetic orientation of cells makes their search for a favorable oxygen concentration more efficient. More than two decades ago, Blakemore et al. (7) demonstrated that the vertical component of the geomagnetic field determines the migration polarity in unidirectional, magnetotactic cells, with South-seeking cells dominating in the Southern Hemisphere and North-seeking cells dominating in the Northern Hemisphere. They proposed that this yields an advantage in seeking an optimal microaerobic environment over several generations.

An efficient tactile response could benefit these bacteria significantly because they are found in environments that can be violently perturbed by flooding as well as changes in the water level (8). That is, bacteria may be forced out of their preferred habitat by mechanical or fluidic forces or their preferred habitat may move. Magnetically oriented bacteria that are displaced should have an advantage because magnetic orientation reduces a three-dimensional search to a one-dimensional search along the magnetic field lines, an inherently more efficient process (9). To our knowledge, this hypothesized magnetic advantage over nonmagnetic cells on a shorter time scale has never been tested. Therefore, we have compared wild-type, magnetic *Magnetospirillum magneticum* AMB-1 (10) (WT) to a nonmagnetic *magA* knockout mutant (DmagA1) with and without applied magnetic fields in the same orientation as an oxygen gradient. Assuming that both magnetic wild-type and nonmagnetic mutant cells have the same oxygen requirements, we show that there is a magnetic advantage in that magnetically oriented cells more efficiently reach the favored microaerobic zone.

MATERIALS AND METHODS

Growth conditions

The basic medium for cultivation of AMB-1 was modified magnetospirillum growth medium (MSGM) containing (per liter): 10 ml Wolfe's vitamin solution, 5 ml Wolfe's mineral solution, 0.68 g (5 mM) potassium phosphate, 0.12 g (1.4 mM) sodium nitrate, 0.035 g (200 μM) ascorbic acid, 0.37 g (2.5 mM) tartaric acid, 0.37 g (3.1 mM) succinic acid, 0.05 g (610 μM) sodium acetate, and 2 ml of 16 mM (33 μM final concentration) ferric quinate. The medium was adjusted to pH 6.75 and autoclaved. The ferric quinate was added after autoclaving. AMB-1 was routinely cultivated on modified MSGM supplemented with 0.1 g yeast extract and 0.2 g polypeptone (per liter). AMB-1 DmagA1 was grown with the addition of kanamycin at 5 μg/ml to maintain selection; however, characterization and magneto-aerotactic experiments were

Submitted March 15, 2006, and accepted for publication May 8, 2006.

Address reprint requests to L. J. Whitman, Tel.: 202-404-8845; E-mail: whitman@nrl.navy.mil.

0006-3495/06/08/1098/10 $2.00

doi: 10.1529/biophysj.106.085167

done without kanamycin. For routine cultivation, cells were grown at 30°C in 15 ml Falcon tubes with minimal head space.

Construction of a nonmagnetic mutant of AMB-1

Disruption of *magA* in AMB-1 has been shown to result in a nonmagnetic phenotype (11). Therefore, a nonmagnetic mutant of AMB-1 was constructed by replacement of the putative *magA* ribosome binding site and the 5′ 659 bp of *magA* with a kanamycin resistance marker (Fig. 1). The delivery vector for the gene replacement construct was pFSP125, a suicide vector derived from pUT (12) by removal of the transposase gene and introduction of unique *Eco*RI, *Eco*RV, *Not*I, and *Bgl*II cloning sites (data not shown). The kanamycin resistance gene from pCR2.1 (Invitrogen, Carlsbad, CA) and its promoter were cloned into pFSP125 along with two flanking sequences amplified by PCR from AMB-1, yielding the gene replacement plasmid pFSP167. Flanking sequence 1 is an 870 bp fragment located 13 bp upstream of *magA*. Flanking sequence 2 consists of the 3′ 646 bp of *magA*. Primers for amplification of the two flanking sequences were designed based on the published sequence of *magA* (11).

The gene replacement suicide plasmid pFSP167 was introduced into AMB-1 by conjugation with the donor strain *Escherichia coli* S17-1 λ*pir* (13). For conjugation, AMB-1 was grown in low iron MSGM (modified MSGM with ferric quinate omitted). S17-1 λ*pir* (pFSP167) was grown in modified MSGM supplemented with 10 mM glucose, 0.1 g yeast extract, and 0.2 g peptone. One half ml of AMB-1 culture was mixed with 0.5 ml of an overnight culture of S17-1 λ*pir* (pFSP167). The mating mix was concentrated by centrifugation in a microfuge at maximum speed for 3 min at 4°C and spotted in 10–30 ml of medium onto solid medium containing modified MSGM, 1% agar, 50 μg/ml sodium thioglycolate, and 10 mM glucose. After overnight incubation at 30°C, the cells were washed from the plate and resuspended in a total volume of 5 ml low iron MSGM. Aliquots of 0.1 ml of mated cells were spread on solid medium containing low iron MSGM supplemented with 1% agar, 50 μg/ml sodium thioglycolate, and 5 μg/ml of kanamycin. Plates were incubated at 30°C for 7–10 days. Isolated colonies were stabbed into a fresh plate of the same medium. Stabs were incubated at 30°C for several days to allow growth of the cells. A stab was excised from the plate and placed in 10 ml of low iron MSGM containing 5 μg/ml kanamycin in a 125 ml screw cap Erlenmeyer flask. The culture was incubated with shaking at 30°C for three weeks until a dense culture had grown.

Transmission-electron microscopy images

Cells were applied to 400-mesh Formvar and carbon-coated Cu grids. Grids were washed by gently moving through water droplets. Unstained cells were imaged using a FEI/Philips CM-10 transmission-electron microscopy operated at 80 kV with spot size 2 and 50 μm objective aperture. Images were captured on Kodak SO-163 film. The magnification of the images was 15,000×.

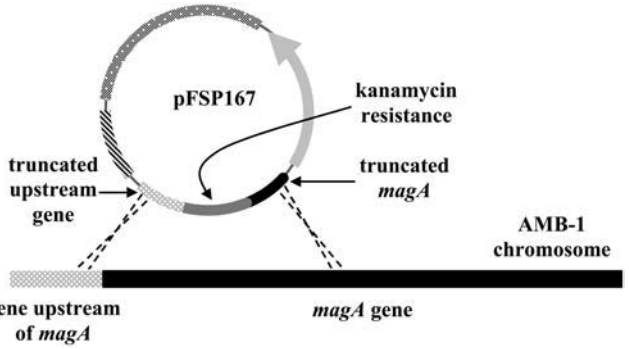

FIGURE 1 Construction of a nonmagnetic mutant of AMB-1 (DmagA1). A suicide plasmid modified with kanamycin resistance marker and promoter, truncated *magA*, and truncated sequence upstream of *magA* were introduced into AMB-1 by homologous recombination.

Growth characterization

Cells were grown as described above, but were sampled by mixing the suspension in the growth tube, opening the tube, and withdrawing a sample with a pipette at each time point. The sample was placed in a masked quartz microcuvette (10 mm path length) and the optical density was measured by absorbance at 470 nm in a Pharmacia (Uppsala, Sweden) Biotech Ultrospec 2000 UV/visible spectrometer. A second sample from the same time point was used to count cells on a Beckman Coulter Multisizer II (Fullerton, CA). A standard curve for cell density versus optical density was produced. The inoculating concentration was measured by viable cell plate counting. A cell sample from the inoculating culture was diluted and grown on a solid support medium containing MSGM supplemented with 0.1 g/L yeast extract, 0.2 g/L polypeptone, 50 mg/L sodium thioglycolate, and 14 g/L agar. Viable plate counting yielded 1×10^7 cfu/ml for the inoculating concentration.

Coefficient of magnetism

A standard, quantitative method for simply and quickly measuring the magnetism of the bacterial population, the coefficient of magnetism (C_{mag}) was measured as previously described (14,15). Briefly, we placed a 25 mm × 25 mm × 12 mm (length × width × depth) neodymium iron boron magnet on top of the lid to the Pharmacia Biotech Ultrospec 2000 UV/visible spectrometer directly over the sample. The magnet was placed so that the magnetic field was parallel or perpendicular to the spectrometer light path. The magnet was ~75 mm from the spectrometer window. The maximum absorbance (magnetic field parallel to light path) was divided by the minimum absorbance (magnetic field perpendicular to light path) at 470 nm to give the C_{mag} value.

Iron uptake measured with ferrozine

Iron uptake was measured as the amount of iron depleted from fresh media by an AMB-1 culture. Cultures were grown in MSGM as described above with 33 μM ferric quinate and 1 ml samples were taken 3 days after inoculation to test for remaining iron. The depleted amount was measured using the iron chelating agent ferrozine (16,17) and by subtracting the remaining iron concentration in spent media from the initial iron concentration in fresh media. The amount of iron depleted from the media was measured by absorbance at 562 nm and normalized to the optical density of cells at 470 nm.

Oxygen response/magnetic advantage experiment

To minimize the introduction of oxygen into the system, cultures were inoculated in rubber septae and crimp-sealed tubing with media in a nitrogen glovebox. Cells were then grown to peak density and tested at 64 h of growth. After referencing a 3 ml sample of sterile medium in an Ocean Optics (Dunedin, FL) S2000 UV/visible spectrometer, a 3 ml sample of cells was retrieved with a syringe and needle and dispensed into a clear quartz cuvette (10 mm path length) within the nitrogen glovebox. The cuvette was capped, removed from the glovebox, and placed in the spectrometer cuvette holder. The cuvette holder was then placed into the center of a pair of Helmholtz coils, which nulled the vertical component of the earth's magnetic field (Fig. 2). To apply a vertical magnetic field, the neodymium iron boron magnet was placed over the cuvette with its magnetic field parallel to the oxygen gradient when specified. Finally, the cuvette was uncapped to allow for oxygen diffusion into the sample while in the spectrometer. The spectrometer window was a 2 mm diameter circle centered 15 mm above the bottom of the cuvette, and the top of the 3 ml cell sample solution was 3.2 cm

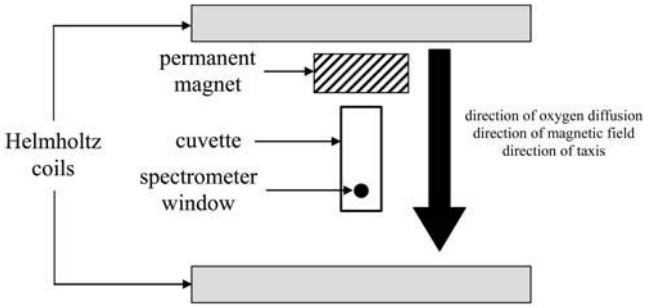

FIGURE 2 Experimental scheme for quantifying magneto-aerotaxis. Note that the spectrometer and cuvette holder are not shown for simplicity. The cuvette is placed in between a pair of Helmholtz coils set to null the vertical component of the earth's magnetic field. A magnetic field is applied by placing a neodymium iron boride magnet (25 mm × 25 mm × 12 mm) close to the cuvette so that the magnetic field is completely vertical at the centerline of the cuvette.

from the bottom of the cuvette. The magnetic field at the sample was 10 G or 150 G, as specified. The spectrometer was set to 300 ms integration time with a Teflon filter on the LS-1-LL Tungsten Halogen light source (Ocean Optics). The spectrometer, a dual channel device, was set to subtract out any time-dependent variations in the intensity of the light source. The spectrometer software (Ocean Optics, OOIBase32) was set to record absorbance at 630 nm at intervals of 1 s (1 Hz) for several hours for most experiments. A few experiments were run at a sampling rate of 0.017 Hz. The changes in optical density, due to aerotaxis, that we tested were on the time scale of hours, therefore a sampling frequency as low as 0.017 Hz was sufficient to capture all the variation of interest.

RESULTS

Genetic engineering and growth characterization

The nonmagnetic mutant strain, DmagA1, was constructed by replacing part of *magA* with a gene encoding kanamycin resistance by homologous recombination with the suicide plasmid pFSP167 (Fig. 1). After introduction of pFSP167 into AMB-1 by conjugation with *E. coli* S17-1 λ*pir*, recombinant AMB-1 were selected for growth on MSGM with kanamycin. One kanamycin resistant recombinant clone was designated DmagA1. The absence of the pFSP167 backbone from DmagA1 was confirmed by sensitivity to ampicillin. The presence of the kanamycin resistance gene was confirmed by PCR.

DmagA1 cells were imaged by electron microscopy to determine the absence of magnetosomes, as shown in Fig. 3. Magnetosomes were present in WT cells, observed as a single chain oriented along the long axis of the cell and stretching ~3/4 of the total length of the cell. Chains consisted of 10–20 30-nm sized particles, sometimes with considerable distance between them (100 nm–1 μm). DmagA1 cells were morphologically similar to WT cells except for the absence of magnetosomes. Moreover, DmagA1 cell populations grew very similarly to WT populations. Both DmagA1 and WT populations grew to peak density in ~40 h after an inoculation with 1×10^7 viable cells/ml, with a peak density of ~1.2×10^8 cells/ml (Fig. 4, and data not shown).

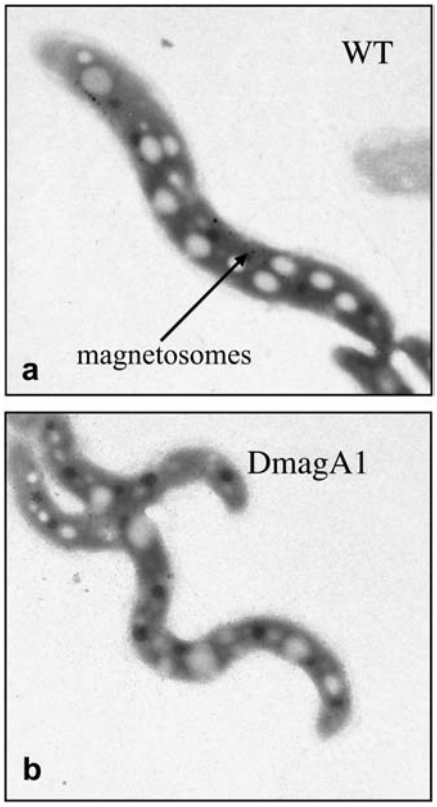

FIGURE 3 Transmission electron microscope images of *M. magneticum AMB-1*. AMB-1 were grown in standard MSGM with 33 μM ferric quinate. AMB-1 WT (*a*) had electron dense regions corresponding to magnetosomes, while DmagA1 were devoid of these electron dense regions (*b*).

Iron uptake and magnetosomes

Cellular iron uptake was determined by measuring iron depletion from the media using ferrozine to detect the iron concentration remaining after 3 days of population growth. Cells took up increasing amounts of iron for increasing initial iron concentrations in the media (Fig. 5 *a*). At lower initial iron concentrations, the population would deplete 100% of the iron in the media, while depleting a smaller percentage when larger concentrations of iron were initially supplied.

Although DmagA1 cells did take up a significant amount of iron, WT cells consistently depleted more iron from the media than DmagA1 cells across all initial iron concentrations. By assuming that the difference in iron uptake between WT and DmagA1 cells was associated with magnetosome formation, it was possible to predict the average magnetic moment per WT cell. The predicted magnetic moment per WT cell, plotted in Fig. 5 *b* (*left axis*), increased with initial iron concentration and plateaued in accordance with the functional measurement of C_{mag} (Fig. 5 *b*, *right axis*). That is, as WT cells were exposed to greater concentrations of iron, their magnetic content increased as measured by C_{mag}. DmagA1 cells maintained a C_{mag} value of 1, indicating no magnetism, for all iron conditions and throughout population

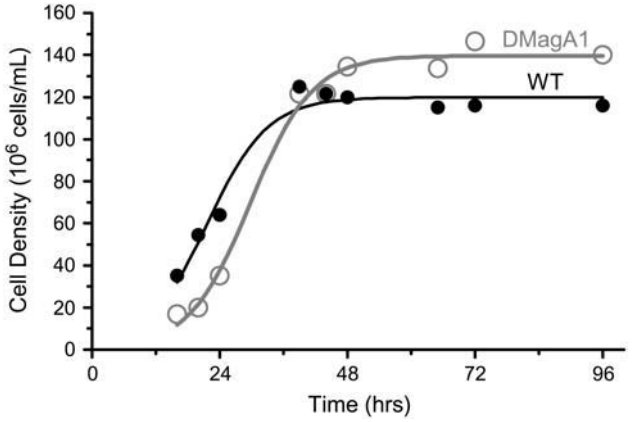

FIGURE 4 Representative curve for cell density during AMB-1 population growth. AMB-1 were grown in MSGM with 33 μM ferric quinate. AMB-1 WT and DmagA1 cultures were inoculated with 1×10^7 viable cells/ml in screw cap tubes with little headspace. Tubes were uncapped and measured in a spectrophotometer for turbidity. DmagA1 grew similarly to WT with a peak in cell density around the two day time point. The solid lines are fits to a logistics curve that return times of maximum growth of 22 $\pm$ 1 h for WT and 30 $\pm$ 1 h for DmagA1.

growth (data not shown). The C_{mag} value for WT cells plateaued at 1.4, which was typical for WT cells in media with iron concentrations of $\sim$30 μM and higher in our setup. At lower iron concentrations, cells presumably formed fewer

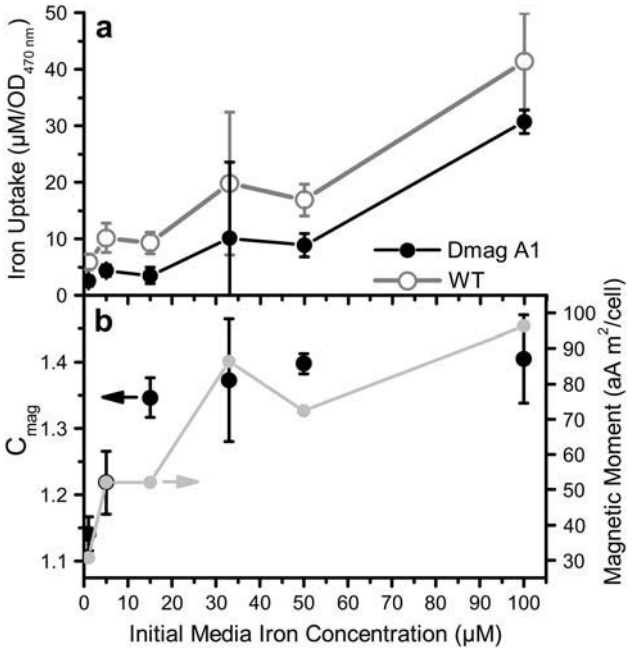

FIGURE 5 (*a*) Iron uptake measured as depletion of iron from the growth media. Iron uptake was normalized by the optical density of the sample at 470 nm and measured at varying initial media iron concentrations. AMB-1 WT (*open circle, shaded line*) accumulated more iron than DmagA1 (*solid circle* and *line*) for all initial concentrations. (*b*) The difference in iron uptake between AMB-1 WT and DmagA1 was plotted as the calculated magnetic moment per cell (*shaded circle* and *line*) and followed the same saturation trend as the C_{mag} measurement (*solid circles* with standard deviation bars) for AMB-1 WT. The correlation between these two data sets is 0.86.

magnetosomes and were less magnetic, resulting in lower C_{mag} values. The predicted magnetic moment plateaued at $\sim 1 \times 10^{-16}$ Am^2/cell (1×10^{-13} emu/cell).

The magnetic moment predicted based on iron uptake is similar to values previously measured by electron holography, light scattering, and vibrating sample magnetometry for another spirillum, *Magnetospirillum magnetotacticum* MS-1 (18–20). Therefore, magnetosome formation in WT cells can be completely accounted for by their increased iron uptake compared to DmagA1 cells. Significantly, *magA* gene disruption in the DmagA1 cells did not completely halt the uptake of iron, with the amount of iron taken up sufficient to maintain cell morphology and motility similar to WT cells (21).

Magneto-aerotactic response: measurements and modeling

AMB-1 cells were placed in a cuvette while in a nitrogen glovebox. Initially, the cell sample was uniformly distributed in the cuvette, and this uniform distribution could be maintained for several hours in a nitrogen environment. Aerotaxis began once the cuvette was uncapped and the sample exposed to atmospheric oxygen. All cells eventually swam to the bottom of the cuvette, escaping the advancing oxygen front. This visually observable migration occurred for both strains with or without an applied magnetic field. The migration rate, however, did depend on the strain and the magnetic field strength.

Cellular migration could be tracked by using the spectrometer to measure the time-dependent optical density which, in turn, is proportional to cell density. Several of these migration curves are shown in Fig. 6. The optical density, read by absorbance in the spectrometer, slowly increased, indicating an accumulation of cells in the spectrometer window as cells migrated away from the high oxygen region at the liquid–air interface toward lower oxygen regions deeper in the cuvette. With time, as the preferred oxygen region passed the spectrometer window, the accumulation of cells reached its peak and then the optical density quickly declined, with very few cells remaining at the level of the spectrometer window. There was often a small additional peak before the decline which is due to low motility cells (as will be discussed below). We attribute the nonzero reading of the spectrometer after the sharp decline in optical density, which persisted for several hours, to some remaining cells which were immotile or dead. As the bacteria approached the bottom of the cuvette and the remaining volume containing the optimal oxygen concentration was compressed, the bacteria formed an observable band that became denser with time; however, this occurred below the field of view in the assay. In addition, the alignment of cells in a magnetic field caused small offset in the measured optical density.

Our modeling of bacterial magneto-aerotaxis is based in part on earlier work by Mazzag et al. (22), which examined bacterial band formation by aerotaxis in *Azospirillum*

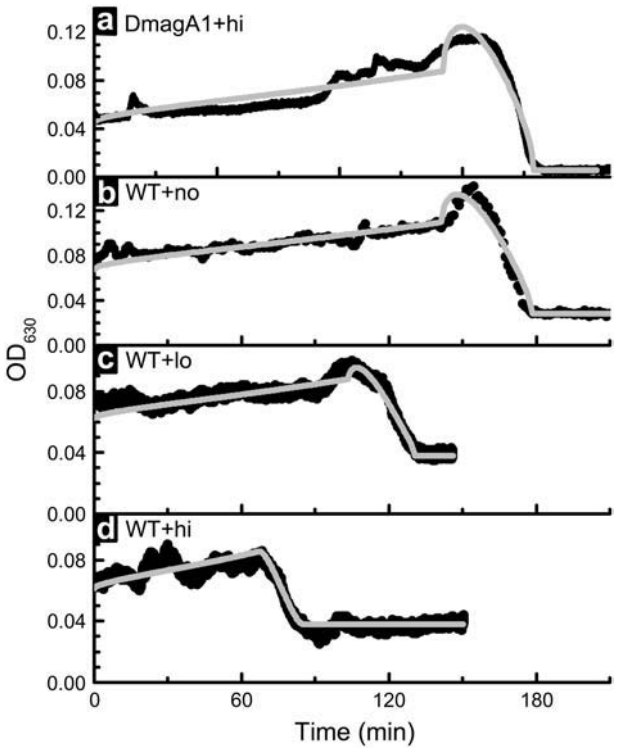

FIGURE 6 Experiment and model (*shaded lines*) of magneto-aerotactic response in an applied magnetic field and oxygen gradient. DmagA1 + hi, WT + hi (150 G vertical field), WT + lo (10 G vertical field), and WT + no (0 G vertical field) initially showed an increase in density caused by aerotaxis and accumulation of cells at the level of the spectrometer window. Then as the preferred oxygen concentration moved below the spectrometer window, most of the cells followed, leaving a very low density of cells behind. WT + hi were more sensitive to the increasing oxygen concentration and so more quickly moved away toward the bottom of the cuvette. As determined from the model fits, the critical oxygen concentration to induce this response, c_{crit}, for WT + hi was exceptionally low (16 nM) because of their magnetic alignment in the direction of the oxygen gradient. In contrast, WT + no and DmagA1 + hi, without assisted alignment, were much less sensitive (higher c_{crit} of 1465 nM and 1494 nM, respectively). WT + lo had an intermediate sensitivity (319 nM).

brasilense. The model system has three components: 1), oxygen, c_{Ox} diffusing down into the cuvette, 2), bacteria swimming up toward the top of the cuvette, T, and 3), bacteria swimming down toward the bottom of the cuvette, B. Both the bacteria swimming up and down move at a constant velocity, v. Velocities for AMB-1 range from 30 to 110 μm/s (23). Finally, depending on the local oxygen concentration, the frequency, f, that the bacteria reverse direction will change. Mathematically, this may be described by

$$\frac{\partial B}{\partial t} = -v\frac{\partial B}{\partial z} - f_{BT}B + f_{TB}T, \quad \frac{\partial T}{\partial t} = v\frac{\partial T}{\partial z} + f_{BT}B - f_{TB}T. \quad (1)$$

A bacterium reaching either the top or bottom of the cuvette will reverse directions such that $B(0) = T(0)$ and $T(L) = B(L)$, where L is the length of the cuvette. These boundary conditions ensure that there is no depletion of bacteria from the cuvette during simulations. At the beginning of the experiment, the inoculation bacteria are evenly divided between T and B and are evenly distributed throughout the cuvette.

The principal challenge in these calculations is the correct determination of the turn frequencies f_{BT} and f_{TB} as a function of oxygen concentration. This process is simpler for magnetotactic bacteria than, for example, *A. brasilense* because magnetotactic bacteria do not appear to seek a desired c_{Ox} by fleeing too high or too low oxygen concentrations (i.e., banding), but rather simply flee if the c_{Ox} is too high. Simulations using the full model described in Eq. 1 showed that a flight response away from low oxygen concentration leads to a distinctive intensity dip before the peak as bacteria move up and out of the detector area and toward the desired oxygen level. Such a dip is not observed experimentally in any of the migration curves (Fig. 6). The implication is that bacteria swimming toward the bottom, B, have a constant, low reversal frequency, f_{lo}. The bacteria swimming toward the top, T, will have the same low reversal frequency as long as the oxygen concentration is below some critical value, c_{crit}. When $c_{Ox} > c_{crit}$, the reversal frequency then increases to f_{hi}:

$$f_{TB} = \begin{cases} f_{lo}, & c_{Ox} < c_{crit} \\ f_{hi}, & c_{Ox} > c_{crit} \end{cases}, f_{BT} = f_{lo}. \quad (2)$$

Observations of the swimming of the bacteria suggest that for healthy bacteria outside a high oxygen area, direction changes are infrequent. In these calculations, we set f_{lo} to 1/(60 s) since higher values do not significantly alter the predicted results. The value for f_{hi} was determined by comparing the simulation to the experimental results as discussed below.

The diffusion of the oxygen into the cuvette may be described by Fick's second law with an added term that accounts for oxygen consumption by the bacteria

$$\frac{\partial c_{Ox}}{\partial t} = D\frac{\partial^2 c_{Ox}}{\partial z^2} - \kappa(T + B), \quad (3)$$

where D is the diffusion coefficient for oxygen in water (2100 $\mu m^2/s$) and κ is the oxygen consumption rate for the bacterium. During the calculation, the consumption term is adjusted such that the oxygen concentration never falls below zero. The description of the oxygen diffusion requires two boundary conditions. We assume that the solution at the meniscus is saturated with oxygen (24) at 256 μM ($= c_{sat}$) and that the bottom of the cuvette is impermeable to oxygen ($\partial c_{Ox}/\partial z(L) = 0$). At the beginning of the experiment, the oxygen concentration in the solution is zero.

The oxygen consumption rate for magnetotactic bacteria is not known. Initially, we assumed the consumption rate $\kappa \sim$ 0.1 fmol/min per cell, in line with that of *A. brasilense*. However, at this value, the bacteria in our model consumed all the diffusing oxygen that would otherwise induce their flight. This effect quickly led to a steady state where the bacteria did not migrate, a clearly incorrect result. Reducing

κ to 1/100th of the initial value led to what appears to be a counterintuitive prediction (Fig. 7): the greater the velocity v of the bacteria, the slower the global response time to the oxygen front. However, this prediction makes sense when one considers that a higher velocity would apply to bacteria heading in both directions (B and T). Specifically, a greater velocity of the T bacteria would allow them to penetrate farther past the point, a, where the oxygen concentration exceeds c_{crit}. By penetrating farther, these bacteria would end up consuming more oxygen before turning and exiting the high oxygen region, which would have the effect of slowing the advance of the oxygen front. A slower advance of the oxygen front, in turn, would lead to a slower overall movement of the bacteria toward the bottom. Experimentally, however, higher magnetic fields lead to greater average bacterial velocities and faster response times. It appears that including any oxygen consumption in the migration simulations produces inaccurate predictions. Given the bacterium's known preference for microaerobic to anaerobic conditions, we therefore conclude that bacterial consumption of oxygen plays a negligible role in the magneto-aerotaxis of AMB-1. Accordingly, the oxygen consumption rate was therefore set to zero ($\kappa = 0$) for the rest of the simulations.

The three remaining model parameters to be addressed are c_{crit}, f_{hi}, and v. The effect of the critical oxygen concentration that initiates migration, c_{crit}, is straightforward (Fig. 8 *a*). Varying this value does not alter the shape of the predicted migration curve, but rather shifts the point in time where it drops to zero. Changing the turnaround frequency, f_{hi}, does not shift the position of the peak intensity (Fig. 8 *b*), but rather low turnaround frequencies create a tail that follows after the peak. Because such tails are not observed in the data (Fig. 6), a relatively high value of f_{hi} is assumed, 1/(4 s), comparable to that for *A. brasilense* (22). Note that higher values do not significantly change the shape of the curve. Changing the velocity of the bacteria, v, also does not shift the time where the migration curve drops to zero, but does significantly change the shape of the curve (Fig. 8 *c*). If the bacteria were to swim faster than the advancing oxygen front ($v > 40$ μm/s, the modal speed for AMB-1 (23))], they would evenly disperse throughout the rest of the cuvette. Thus, the number of bacteria in the detector area would slowly increase as bacteria fleeing the oxygen front enter. However, when the oxygen front eventually enters the detector area, the bacteria would be expelled, leading to a rapid drop in the predicted migration curve. If v were less than the speed of the oxygen front—which is 30 μm/s at 30 min, but decreases $\propto 1/\sqrt{t}$ to 8 μm/s at 180 min—then the bacteria would be swept along by the moving oxygen front and would form a band (25–27). Examining the experimental results in Fig. 6, it is apparent from the shapes of the curves that the majority of the bacteria are moving faster than the oxygen front. However, there is a pronounced peak for several of the curves; that is, there appears to be at least two populations, one fast and one slow, that are reacting to the oxygen front.

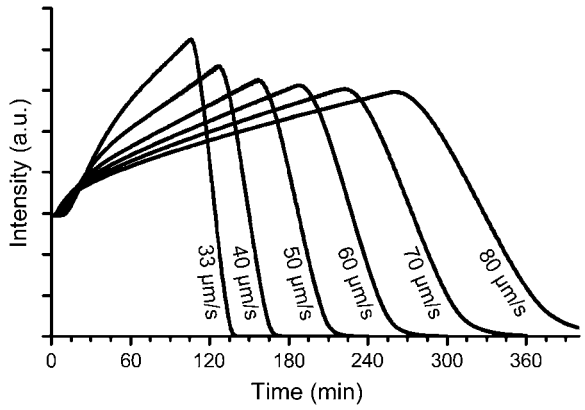

FIGURE 7 Simulated migration curves when oxygen consumption by the bacteria is included in the model. In this simulation set, the bacteria swim at the stated velocity with $c_{crit} = 21$ nM and $f_{hi} = 1/(4\text{ s})$. These results simulate the migration if they were to consume even 1/100th the amount of oxygen as would *A. brasilense* (~0.1 fmol/(min·cell)). Notably, greater velocities increase the penetration of the bacteria into the high oxygen regions, where they consume greater oxygen before leaving, thereby slowing the advance of the oxygen front and the associated migration of the bacteria.

Summarizing our model, the three main characteristics of the simulations are 1), the value of c_{crit} shifts the peak time, 2), the bacteria respond quickly to the oxygen front, and 3), there appears to be a fast population and a slow population. Using these results, the model may be sufficiently simplified to enable fitting to the data while retaining the simulation's crucial characteristics. Our simplified model assumes that the fast population reacts sufficiently fast that any bacteria displaced by the advancing front are evenly distributed through the remainder of the cuvette, and that the slow population exists as a single pulse (i.e., a delta function) at the position of the oxygen front, a. Mathematically, this can be described by

$$\text{Intensity} = \begin{cases} p_{\text{fast}}\frac{L}{L-a}, & a < x_0 - R \\ p_{\text{fast}}\frac{2L}{\pi R(L-a)}\int_a^{x_0+R}\sqrt{1-\left(\frac{x-x_0}{R}\right)^2}dx + (1-p_{\text{fast}})\sqrt{1-\left(\frac{a-x_0}{R}\right)^2}, & x_0 - R < a < x_0 + R \\ 0, & a > x_0 + R \end{cases}, \tag{4}$$

where p_{fast} is the fractional population of fast bacteria, x_0 is the distance to the center of the detector (17.5 mm), and R is the radius of the detector (1 mm). The location of the diffusion front, a, is calculated using the solution to Eq. 3 with $\kappa = 0$:

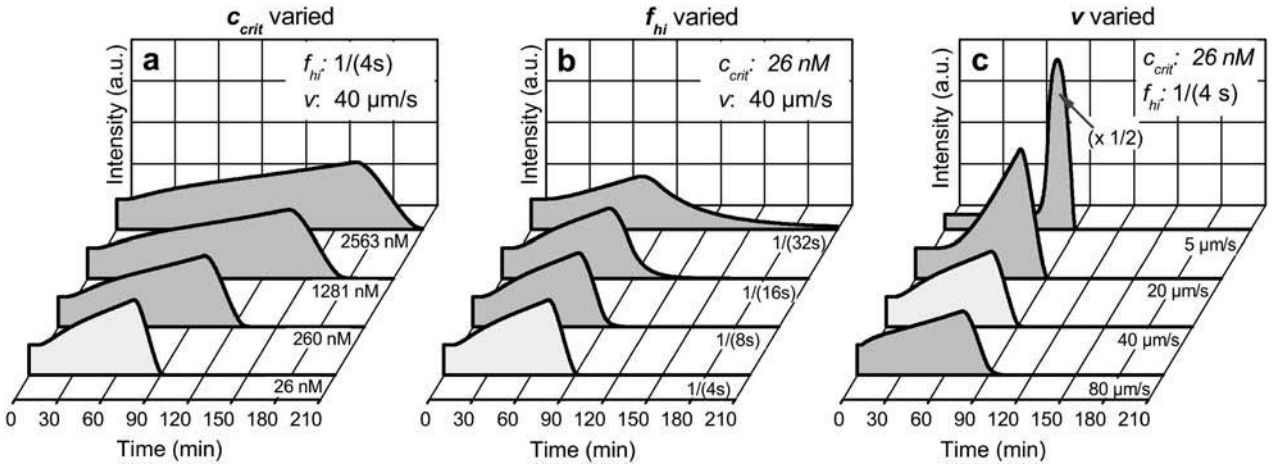

FIGURE 8 Change in simulated migration curves as the critical parameters—c_{crit}, f_{hi}, and v—are varied in the case where no oxygen is consumed. Note that the light shaded curve is identical in each plot. (*a*) Lower values of c_{crit} shift the position of the peak to shorter times indicating a faster response by the bacteria. (*b*) A lower high turnaround frequency, f_{hi}, leads to longer tails after the peak. Minimal tails are observed experimentally. (*c*) Lower bacterial velocities, v, lead to sharper peaks.

$$a = 2\sqrt{Dt} \times ierfc\left(\frac{c_{crit}}{c_{sat}}\right), \tag{5}$$

where *ierfc* is the inverse complementary error function. Fits using this formula were performed in MathCad 13 and are shown in Fig. 6. (Technically, this is the solution for an infinitely deep cuvette; however, the location of the detector window is sufficiently far from the cuvette bottom that there is no discernible difference between this solution and the more complicated but exact solution during the experimental time frame.)

Fitting our data to this model, we compared WT cell migration in the presence of a high vertical magnetic field (WT + hi) and a low vertical magnetic field (WT + lo) to migration without any vertical field (WT + no). Representative plots and fits for several comparisons are shown in Fig. 6 and the associated values shown in Table 1. WT cells in a high magnetic field migrated significantly faster than in any other scenario, responding at a c_{crit} of 21 ± 5 nM (Table 1). By comparison, WT in no vertical magnetic field had the slowest response, responding only at a c_{crit} of 1393 ± 102 nM; a concentration 66 times higher than observed in a high magnetic field. The significantly ($P \ll 0.01$) lower c_{crit} for WT + hi over that for WT + no quantitatively shows the advantage provided by magneto-aerotaxis over aerotaxis. Decreasing the magnitude of the magnetic field (WT + lo) reduces the effectiveness of the response, such that its c_{crit} of 299 ± 244 nM lies between the high and no field experiments (Fig. 6, Table 1). The c_{crit} for WT + lo remains significantly higher than WT + hi ($P = 0.06$) and less ($P < 0.01$) than WT + no.

We hypothesize that the response of DmagA1 cells with or without a vertical magnetic field should be similar to WT + no, assuming the disturbance of *magA* and magnetosome formation did not dramatically affect oxygen sensitivity. Testing DmagA1 cells in no field (DmagA1 + no), gave a c_{crit} of 809 ± 506 nM, whereas the c_{crit} for DmagA1 + hi (150 G vertical field) was 532 ± 565 nM. These concentrations are not significantly different ($P = 0.53$), so the values for both cases were pooled for comparison to the WT data. The average c_{crit} for the pooled DmagA1 data was 671 ± 562 nM. Although the standard deviation in c_{crit}, which is related to the population's time response, appears high, it is consistent with and on the same order as the standard

TABLE 1 Quantitative fits of the magneto-aerotactic response in an applied magnetic field and oxygen gradient for both wild-type (WT) and DmagA1 non-magnetic knock-outs

Vertical magnetic Field (*G*)	p_{fast} (%)		c_{crit} (*nM*)		t_{cen} (min)	
	WT	DmagA1	WT	DmagA1	WT	DmagA1
150	74 ± 29	60 ± 28	21 ± 5	532 ± 655	78	128
10	64 ± 6	ND	299 ± 244	ND	116	ND
0	55 ± 2	55 ± 12	1393 ± 102	809 ± 506	157	138

The fraction that responds quickly, p_{fast}, (mean ±SD) and the critical oxygen concentration for inducing flight, c_{crit}, were calculated according to the model described in the text. The average time at which the oxygen front passed the detector center, t_{cen}, was calculated. The fast fraction decreased with long migration times. WT cell migration varied strongly with magnetic field. The migration times for DmagA1 were statistically independent of magnetic field. (ND, not determined.)

deviation in swimming speed (23). (Small standard deviations in closely grouped, magnetotactic cells could be caused by synchronized swimming due to hydrodynamic coupling (26).) Comparing the pooled DmagA1 data to the WT + no data, we found a small statistical difference ($P = 0.12$) in c_{crit}. The average c_{crit} for the DmagA1 data was 42% less than the WT + no data, suggesting there may be a subtle coupling between *magA* function or magnetosome formation and oxygen tolerance. It should be noted that DmagA1 still responds to oxygen gradients after the *magA* gene has been knocked out, suggesting that the sensing and response mechanisms remain intact. Significantly, comparison of the pooled DmagA1 data to the WT + hi data showed that c_{crit} was substantially less for WT + hi ($P = 0.04$), indicating that *m*agneto-aerotaxis allows more efficient migration than aerotaxis alone. In all cases, the inability to orient along the direction of the applied oxygen gradient via magnetic field resulted in a slower aerotactic response. The critical oxygen concentration to induce a response for cells able to orient in a magnetic field was at least 66 times lower (WT + hi) and 4.7 times lower (WT + lo) than for nonorienting cells, WT + no, demonstrating the magnetic advantage.

In addition to inducing migration, the population shifts determined by the fits suggest that oxygen exposure also impairs the mobility of the bacteria. From Table 1, it is apparent that the time required for the oxygen front to pass the center of the detector, t_{cen}, and the fraction of active bacteria, p_{fast}, are correlated (corr $= -0.97$). That is, longer exposure to oxygen decreases the fraction of bacteria with high motility. Given our own observations and those by Seong et al. (23) that aerobically grown bacteria have low motility, and given AMB-1's preference for low oxygen levels, it appears that exposure to oxygen decreases their motility.

DISCUSSION

The concerted orientation and migration of magnetotactic bacteria following magnetic field lines is a visually stunning display. The ecological significance of the coupling of magnetic orientation with aerotaxis has been presumed to be great and a matter of survival. Although the *M. magneticum* AMB-1 used in this study can grow aerobically, they prefer a microaerobic environment (10). AMB-1 cultures grown aerobically can include cells with an abnormal, spherical appearance (possibly spheroplasts). Aerobically grown AMB-1 cells also exhibit much reduced motility (by microscopic observation), and a shorter population lifetime compared to microaerobically grown cells (data not shown). Taking into consideration the impaired aerobic growth of AMB-1 and the more severe consequences of aerobic growth in other species (28), there appears to be a clear selective pressure for their microaerobic mode of growth. Their survival then hinges on an efficient search for a less oxygenated environment when their preferred, natural environment is disturbed, as can be the case, for example, for environments with seasonal water table variations including tides (8). The focus of our study was to determine and quantify a magnetic advantage in bipolarly flagellated magnetotactic bacteria.

To quantify the magnetic advantage, we varied the magnetic contribution to aerotactic cell migration in two ways. First, we nulled the magnetic field in the direction of aerotactic migration with Helmholtz coils. This allowed WT, magnetic cells to respond to an oxygen gradient without a bias on their orientation in the direction of the gradient. Second, we produced a nonmagnetic AMB-1 cell type by knocking out the *magA* gene, producing the magnetosome-free strain DmagA1. These DmagA1 cells did not preferentially orient with respect to any magnetic field, while displaying similar growth characteristics to the WT. Although, DmagA1 cells still took up significant amounts of iron, their iron uptake was decreased compared to WT cells; this difference was well accounted for by the quantity of iron theoretically incorporated into magnetosomes, according to magnetic moment calculations. Overall, DmagA1 cells appeared similar to WT cells except for their decreased iron uptake and lack of magnetosomes.

The DmagA1 cells responded to an oxygen gradient challenge in a similar fashion to WT cells when there was zero magnetic field in the direction of the gradient. Without the magnetic advantage of alignment parallel to the gradient, aerotaxis took more than 2.5 h in our experiments, compared to half that time for magnetically assisted aerotaxis of the WT. An intermediate field strength provided an intermediate enhancement for the WT. Using our procedure, we did not observe any measurable enhancement with low magnetic fields comparable to the earth's. Our experimental method was not sensitive enough to quantify the difference in response between WT cells in no field and WT cells in the earth's field given a relatively limited number of measurements and the natural variance. The geomagnetic field may have an observable effect in this assay on a longer time and distance scale than was studied here. As the geomagnetic field is relatively weak compared to field strengths used in this study and the viability of a single AMB-1 cell can ensure population survival, high resolution measurements and observations might be required to better quantify the geomagnetic contribution to magnetotactic bacterial survival. This result implies that the environmental effect of the earth's field on AMB-1 magneto-aerotactic response must be very subtle, but still significant enough to enhance survival.

Modeling the magneto-aerotaxis generated several insights into the behavior of the bacteria. First, we find that AMB-1, unlike *A. brasilense*, does not have a preferred range of oxygen concentrations but rather has only an upper limit, c_{crit}, at which they flee. Second, it is clear that magnetic alignment enhances the sensitivity of the bacteria to oxygen (lowering this limit). One could envision that magnetic alignment would enhance a bacterium's flight from high oxygen either by increasing its flight velocity or by somehow enhancing its ability to sense oxygen (and/or the oxygen gradient). Magnetic alignment could increase the flight velocity by

counteracting the Brownian forces that might otherwise deflect the bacteria in its flight from the oxygen front, as follows. Consider two populations of bacteria moving at the same speed downwards—one population where all bacteria are perfectly aligned along the z axis, and one population where the directions of the bacteria are randomly distributed through the downward angles. The average velocity, $\langle v_{un} \rangle$, of the unaligned bacteria would be half that of the aligned bacteria:

$$\langle v_{un} \rangle = \frac{2}{\pi v^2} \int_0^{\pi/2} \int_0^{\pi/2} (v \times \cos(\theta)) v^2 \sin(\theta) d\theta d\phi = \frac{v}{2}. \quad (6)$$

Alternately, greater oxygen sensitivity could arise from the path of an upward-moving bacterium being more aligned with the oxygen gradient. An aligned bacterium would see an average increase in oxygen concentration with time that was twice that for the unaligned bacteria. (An analogy would be a hiker either climbing straight up a mountain or climbing back and forth along a switchback trail; climbing straight up a mountain produces a greater climbing rate.) Given that bacteria are known to use temporal comparisons of concentrations when deciding whether to turn around (29), such path alignment could have a significant impact on their ability to detect oxygen (It should be noted that these simulations cannot differentiate between sensitivity to oxygen concentration and sensitivity to the gradient of the oxygen concentration. The concentration and the concentration gradient are monotonically related such that, mathematically, sensitivity to one implies sensitivity to the other. It is assumed that the biologically relevant value is the oxygen concentration and so the increase in sensitivity is reported in those terms.)

Our results and simulations indicate that only this second mechanism, path alignment, enhances the flight from oxygen; that is, the magnetic advantage stems from a greater ability to detect the oxygen concentration rather than a faster flight away from high oxygen concentrations. At this stage, it is unclear why the advantage is so pronounced. Given that the aligned bacteria experience an average rate change in oxygen concentration that is no greater than twice that of the unaligned bacteria, how is an increase in sensitivity of 66 times obtained? One possibility is that the biochemical mechanism for detecting changes in oxygen concentration is itself regulated by the rate of change, providing amplification to the sensing efficiency. Additionally, given that an increased alignment of the bacteria (through increased magnetic fields) increases their oxygen sensitivity, one could speculate that there is an evolutionary balance between the number of magnetosomes, the local magnetic field strength, and the required sensitivity to oxygen.

CONCLUSIONS

In conclusion, we have quantitatively compared the magnetically-enhanced aerotaxis of wild-type, magnetic *M. magneticum* AMB-1 with a nonmagnetic mutant we have engineered from this strain. Using an applied magnetic field and an advancing oxygen gradient, we have quantified the magnetic advantage in magneto-aerotaxis as a more rapid migration to preferred oxygen levels. Magnetic, wild-type cells swimming in an applied magnetic field more quickly migrate away from the advancing oxygen than either wild-type cells in a zero field or the nonmagnetic mutants in any field. We find that the responses of these different strains can be well described using a relatively simple analytical model, an analysis of which indicates that the key benefit of magnetotaxis is the enhancement of a bacterium's ability to detect oxygen, not an increase in its average speed moving away from high oxygen concentrations. That is, the magnetic advantage is caused by an increased ability to sense oxygen concentration as opposed to faster taxis. Finally, we also observe that during taxis there is a population shift from high to low motility bacteria, most likely caused by damage from oxygen exposure.

This work was supported by the DARPA BioMagnetICs program. M.S. was supported by an American Society for Engineering Education Fellowship at the Naval Research Laboratory.

REFERENCES

1. Frankel, R. B., and R. P. Blakemore. 1980. Navigational compass in magnetic bacteria. *J. Mag. Mag. Mat.* 15–18:1562–1564.
2. Schuler, D., and E. Baeuerlein. 1998. Dynamics of iron uptake and Fe3O4 biomineralization during aerobic and microaerobic growth of Magnetospirillum gryphiswaldense. *J. Bacteriol.* 180:159–162.
3. Yang, C. D., H. Takeyama, T. Tanaka, and T. Matsunaga. 2001. Effects of growth medium composition, iron sources and atmospheric oxygen concentrations on production of luciferase-bacterial magnetic particle complex by a recombinant Magnetospirillum magneticum AMB-1. *Enzyme Microb. Techol.* 29:13–19.
4. Blakemore, R. P. 1982. Magnetotactic bacteria. *Annu. Rev. Microbiol.* 36:217–238.
5. Bazylinski, D. A., and R. B. Frankel. 2004. Magnetosome formation in prokaryotes. *Nat. Rev. Microbiol.* 2:217–230.
6. Schuler, D. 1999. Formation of magnetosomes in magnetotactic bacteria. *J. Mol. Microbiol. Biotechnol.* 1:79–86.
7. Blakemore, R. P., R. B. Frankel, and A. J. Kalmijn. 1980. South-seeking magnetotactic bacteria in the Southern Hemisphere. *Nature.* 286:384–385.
8. Mann, S., N. H. Sparks, and R. G. Board. 1990. Magnetotactic bacteria: microbiology, biomineralization, palaeomagnetism and biotechnology. *Adv. Microb. Physiol.* 31:125–181.
9. Frankel, R. B., and R. P. Blakemore. 1989. Magnetite and magnetotaxis in microorganisms. *Bioelectromagnetics.* 10:223–237.
10. Matsunaga, T., T. Sakaguchi, and F. Tadokoro. 1991. Magnetite formation by a magnetic bacterium capable of growing aerobically. *Appl. Microbiol. Biotechnol.* 35:651–655.
11. Nakamura, C., J. G. Burgess, K. Sode, and T. Matsunaga. 1995. An iron-regulated gene, magA, encoding an iron transport protein of Magnetospirillum sp. strain AMB-1. *J. Biol. Chem.* 270:28392–28396.
12. Herrero, M., V. de Lorenzo, and K. N. Timmis. 1990. Transposon vectors containing non-antibiotic resistance selection markers for cloning and stable chromosomal insertion of foreign genes in gram-negative bacteria. *J. Bacteriol.* 172:6557–6567.
13. de Lorenzo, V., I. Cases, M. Herrero, and K. N. Timmis. 1993. Early and late responses of TOL promoters to pathway inducers: identification

of postexponential promoters in Pseudomonas putida with lacZ-tet bicistronic reporters. *J. Bacteriol.* 175:6902–6907.

14. Schuler, D., R. Uhl, and E. Bauerlein. 1995. A simple light scattering method to assay magnetism in Magnetospirillum gryphiswaldense. *FEMS Microbiol. Lett.* 132:139–145.
15. Komeili, A., H. Vali, T. J. Beveridge, and D. K. Newman. 2004. Magnetosome vesicles are present before magnetite formation, and MamA is required for their activation. *Proc. Natl. Acad. Sci. USA.* 101: 3839–3844.
16. Carter, P. 1971. Spectrophotometric determination of serum iron at the submicrogram level with a new reagent (ferrozine). *Anal. Biochem.* 40: 450–458.
17. Stookey, L. L. 1970. Ferrozine–a new spectrophotometric reagent for iron. *Anal. Chem.* 42:779–781.
18. Dunin-Borkowski, R. E., M. R. McCartney, R. B. Frankel, D. A. Bazylinski, M. Posfai, and P. R. Buseck. 1998. Magnetic microstructure of magnetotactic bacteria by electron holography. *Science.* 282: 1868–1870.
19. Rosenblatt, C., F. F. Torres de Araujo, and R. B. Frankel. 1982. Light scattering determination of magnetic moments of magnetotactic bacteria. *J. Appl. Phys.* 53:2727–2729.
20. Denham, C. R., R. P. Blakemore, and R. B. Frankel. 1980. Bulk magnetic properties of magnetotactic bacteria. *IEEE Trans. Magn.* 16:1006–1007.
21. Nakamura, C., Y. Hotta, R. H. Thornhill, and T. Matsunaga. 1995. Characterization of nonmagnetic mutant of Magnetospirillum sp. strain AMB-1. *J. Mar. Biotechnol.* 3:97–100.
22. Mazzag, B. C., I. B. Zhulin, and A. Mogilner. 2003. Model of bacterial band formation in aerotaxis. *Biophys. J.* 85:3558–3574.
23. Seong, S., and T. H. Park. 2001. Swimming characteristics of magnetic bacterium, Magnetospirillum sp. AMB-1, and implications as toxicity measurement. *Biotechnol. Bioeng.* 76:11–16.
24. Weiss, R. F. 1970. The solubility of nitrogen, oxygen, and argon in water and seawater. *Deep Sea Research.* 17:721–735.
25. Spormann, A. M., and R. S. Wolfe. 1984. Chemotactic, magnetotactic and tactile behaviour in a magnetic spirillum. *FEMS Microbiol. Lett.* 22:171–177.
26. Guell, D. C., H. Brenner, R. B. Frankel, and H. Hartman. 1988. Hydrodynamic forces and band formation in swimming magnetotactic bacteria. *J. Theor. Biol.* 135:525–542.
27. Spormann, A. M. 1987. Unusual swimming behavior of a magnetotactic bacteria. *FEMS Microbiol. Ecol.* 45:37–45.
28. Blakemore, R. P., D. Maratea, and R. S. Wolfe. 1979. Isolation and pure culture of a freshwater magnetic spirillum in chemically defined medium. *J. Bacteriol.* 140:720–729.
29. Berg, H. C. 1983. Random Walks in Biology. Princeton University Press, Princeton, NJ.